Photochemistry

DOI: 10.1002/anie.201205995

Photonic Engineering of Hybrid Metal–Organic Chromophores**

Mickaël P. Busson, Brice Rolly, Brian Stout, Nicolas Bonod, Jérôme Wenger, and Sébastien Bidault**

Fluorescent probes play a key role in sensing, imaging, and energy harvesting. A common element found among the wide library of existing chromophores is that their photophysical responses have been designed following a molecular engineering approach that tunes the electronic and vibrational eigenstates of the molecules.[1–4] A conceptually different approach is to tailor the molecular photophysical response through the external electromagnetic field, which we call photonic engineering. As pioneered by K. H. Drexhage with Eu^{3+} complexes in the vicinity of a mirror,[5] different luminescence properties can be engineered electromagnetically by changing the local density of optical states (LDOS):[6,7] the emission rates, excitation cross-sections, and quantum yield of dye molecules, as well as spectroscopic selection rules (electric/magnetic dipolar/quadrupolar transitions) or intersystem-crossing rates. Despite the intense recent research on fluorophores coupled to photonic structures,[8–18] one of the main practical features of traditional chromophores, their solubility, remains a challenge. Indeed, a practical implementation of the photonic engineering approach requires combining, in a single hybrid nanostructure, a luminescent molecule and an optical antenna or cavity that confines the electromagnetic field.[19]

Herein, we experimentally demonstrate control of the absorption and emission properties of individual emitters by photonic antennas in suspension. The method results in a new class of water-soluble chromophores with unprecedented photophysical properties, such as short lifetime, low quantum yield but high brightness. We study purified suspensions of 40 nm diameter gold nanoparticles (AuNP) monomers and dimers linked to a single 30 or 50 base pair (bp) DNA double-strand exhibiting a single ATTO647N molecule, as recently demonstrated by our group.[20,21] A combination of fluorescence correlation spectroscopy (FCS), time-correlated fluorescence measurements and spectroscopy fully characterizes these hybrid metal–organic emitters by their absorption cross-sections, fluorescence lifetimes, quantum yields, and translational and rotational diffusion coefficients. These measurements also assess the high purity of the functionalized AuNP samples with negligible free dyes and weak monomer subpopulations ($<30\,\%$) in dimer samples. Compared to isolated chromophores, an organic dye engineered by a AuNP dimer exhibits absorption cross-sections and spontaneous decay rates enhanced by more than one order of magnitude without losing its brightness.

Noble-metal nanostructures, that exhibit broad resonant excitations of their valence electrons (plasmon), offer the combination of enhanced local fields and large scattering cross-sections needed to strongly influence the absorption and emission properties of chromophores.[8–13] Nanoparticle dimers are particularly attractive as the electromagnetic field is strongly confined in the nanometer gap that separates the particles.[14] In Purcell factor terms, the strong field confinement compensates the weak quality factor of the plasmon resonance.[22] Using electrophoresis, we synthesize gold nanoparticle dimers linked by a single DNA double-strand, that are stretched by repulsive electrostatic interactions.[20] The interparticle distance is tuned by changing the length of the DNA template, and a single ATTO647N molecule is introduced in the structure.[21] Figure 1 a represents the considered nanostructure geometry and Figure 1 b provides a typical cryo-electron microscopy (cryo-EM) image of 40 nm AuNPs linked by a single 50 bp DNA strand. We consider five different sample geometries: a reference solution of ATTO647N modified 50 bp DNA strands (ATTO), suspensions of single 40 nm diameter AuNPs functionalized with one ATTO647N modified 50 bp or 30 bp DNA strand (mono50 and mono30, respectively) and suspensions of 40 nm AuNP dimers linked by a single ATTO647N modified 50 bp or 30 bp DNA linker (dim50 and dim30).

To demonstrate photonic engineering of water-soluble chromophores, we investigate the sample suspensions with FCS, time-correlated fluorescence measurements and spectroscopy. FCS is a powerful method to accurately quantify the average number of emitters in the confocal detection volume and their average brightness, and infer the sample translational and rotational diffusion properties.[23–25] Fluorescence correlation functions for the ATTO, mono30, and dim30 samples are shown on Figure 1 c for a linearly polarized excitation. These data are normalized to better reveal the changes in the correlation times (raw data are provided in the

[*] M. P. Busson, Dr. S. Bidault
Institut Langevin, ESPCI ParisTech, CNRS UMR 7587
INSERM U979, 1 rue Jussieu, 75005 Paris (France)
E-mail: sebastien.bidault@espci.fr
B. Rolly, Dr. B. Stout, Dr. N. Bonod, Dr. J. Wenger
Institut Fresnel, CNRS, UMR 7249, Aix-Marseille Université
Ecole Centrale Marseille
Campus de Saint Jérôme, 13397 Marseille (France)
E-mail: jerome.wenger@fresnel.fr

[**] The authors thank E. Larquet for the cryo-electron microscopy measurement. The research leading to these results has received funding from the Agence Nationale de la Recherche through grant number ANR 11 BS10 002 02, and the European Research Council under the European Union's Seventh Framework Programme (grant number FP7/2007-2013)/ERC grant agreement 278242. Work at the Institut Langevin is supported by the Laboratoire d'Excellence (LabEx) WIFI.

Supporting information for this article is available on the WWW under http://dx.doi.org/10.1002/anie.201205995.

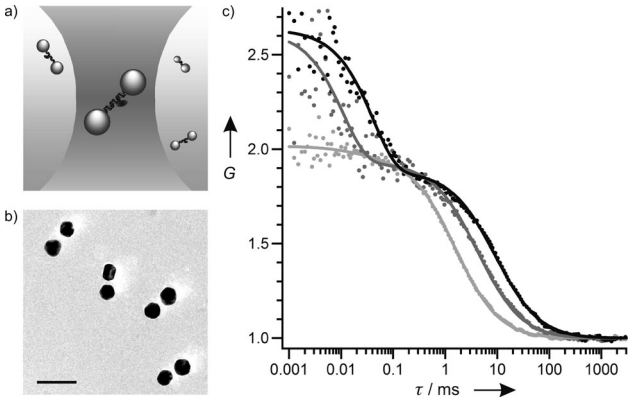

Figure 1. a) DNA-templated AuNP dimers as water-soluble hybrid metal–organic chromophores. b) Cryo-EM image of 50 bp DNA-templated 40 nm AuNP dimers (dim50, the scale bar is 100 nm). c) Normalized FCS correlation functions (G) versus the lag time (τ) for the reference ATTO647N-DNA sample (ATTO, light grey), 30 bp monomers (mono30, grey), and 30 bp dimers (dim30, black). The points correspond to experimental data and the solid lines to a numerical fit.

Supporting Information for all sample geometries). Numerical fitting of the FCS data is based on a standard three-dimensional Brownian diffusion model for single species assuming Gaussian excitation and detection mode profiles (see the Supporting Information for details).[25] Two different characteristic times are readily seen in the FCS data: the long timescale denotes translational diffusion, while the timescale below 100 μs relates to rotational diffusion of the metal–organic chromophores respective to the laser linear polarization.

Table 1 summarizes the translational and rotational diffusion times as well as the translational diffusion coefficients and hydrodynamic radii derived from the diffusion times. Values obtained for the reference ATTO sample are consistent with a 50 bp DNA double-strand, and gradually increase when adding one or two AuNPs. This behavior further confirms the purity of our monomer and dimer suspensions. The number of free dyes in the monomer samples is estimated below 5% and negligible for the dimers. Lastly, we infer theoretically the correlation times induced by rotational diffusion for a single sphere and a prolate ellipsoidal particle to mimic the dimer (last column of Table 1).[26] The good agreement with our experimental data confirms that the plateau observed in the FCS correlation functions below 100 μs relates to rotational diffusion, and not to triplet blinking.

Table 1: Diffusion properties of hybrid metal–organic chromophores.

Sample	Diffusion time [ms]	Diffusion coefficient [$cm^2 s^{-1}$]	Hydrodynamic radius [nm]	Rotational time [μs]	Rotational time [μs] (theory)
ATTO	1.53 ± 0.05	5.3×10^{-7}	4.1	–	–
mono50	4.3 ± 0.1	1.9×10^{-7}	11.5	11 ± 1	11[a]
mono30	4.2 ± 0.1	1.9×10^{-7}	11.3	11 ± 1	11[a]
dim50	9.6 ± 0.2	8.5×10^{-8}	25.7	36 ± 2	36.9[b]
dim30	9.2 ± 0.2	8.8×10^{-8}	24.6	38 ± 2	33.4[c]

[a] 44 nm diameter sphere. [b] 40 nm wide, 99 nm long prolate ellipsoid. [c] 40 nm wide, 93 nm long prolate ellipsoid.

A key parameter for applications is the fluorescence brightness, quantified by the average number of photons detected per chromophore. This value is readily obtained by dividing the average fluorescence intensity by the average number of emitters measured by FCS. Figure 2a presents the molecular brightness as a function of the excitation intensity, and Table 2 summarizes the fluorescence enhancement as compared to the reference ATTO sample in the excitation regime below 65 $\mu W\,\mu m^{-2}$. Remarkably, 30 bp AuNP dimers provide 1.35 times more signal than the reference ATTO sample, while for all other sample geometries the brightness is quenched as compared to the reference. Please note that these values are time-averaged and spatially averaged over all positions and orientations inside the confocal volume; for some given positions and orientations, the fluorescence enhancement can be much higher. Statistical analysis of cryo-EM images of dimers indicates that 30 bp and 50 bp linkers correspond to (13 ± 2) and (17.5 ± 3) nm, respectively.[20] Therefore, we only observe enhancement of the fluorescence signal for a single molecule in 40 nm AuNP dimers when the emitter–particle distance falls below 8 nm: enhancement by a factor of 1.35 at about 6.5 nm compared to a factor of 0.76 at about 9 nm. For monomer samples, the distance dependence of the enhancement factor is reversed: the brightness is divided by about three at an emitter–particle distance (mono30) of about 6.5 nm while it is only divided by about two at about 9 nm (mono50).

Table 2: Photophysical properties of hybrid metal–organic emitters.

Sample	Fl. enhancement factor[a]	τ [ps]	ε [$M^{-1} cm^{-1}$] @633 nm	ϕ [%]
ATTO	1	4300 ± 100	10^5[b]	65[c]
mono50	0.51 ± 0.01	615 ± 20	$(3.4 \pm 0.4) \times 10^5$	9.3 ± 1.0
mono30	0.35 ± 0.01	135 ± 15	$(12 \pm 2) \times 10^5$	1.8 ± 0.3
dim50	0.76 ± 0.02	185 ± 15	$(11 \pm 1.5) \times 10^5$	4.8 ± 0.7
dim30	1.35 ± 0.04	65 ± 10	$(57 \pm 9) \times 10^5$	1.6 ± 0.3

[a] Estimated in the linear, low excitation regime, with respect to ATTO; Fl. = fluorescence. [b] Extrapolated at 633 nm. [c] As provided by the manufacturer for free ATTO647N in water.

To verify that these signal evolutions are not due to a chemical modification of the luminescent emitter, we measure the fluorescence spectra for the different samples on Figure 2b. All spectra are normalized by the average number of emitters quantified by FCS, and indicate quantitatively the same enhancement and quenching factors as in Figure 2a. Most importantly, all spectra are centered on 670 nm as expected for ATTO647N fluorescence, indicating that the emitter-antenna interaction does not modify the

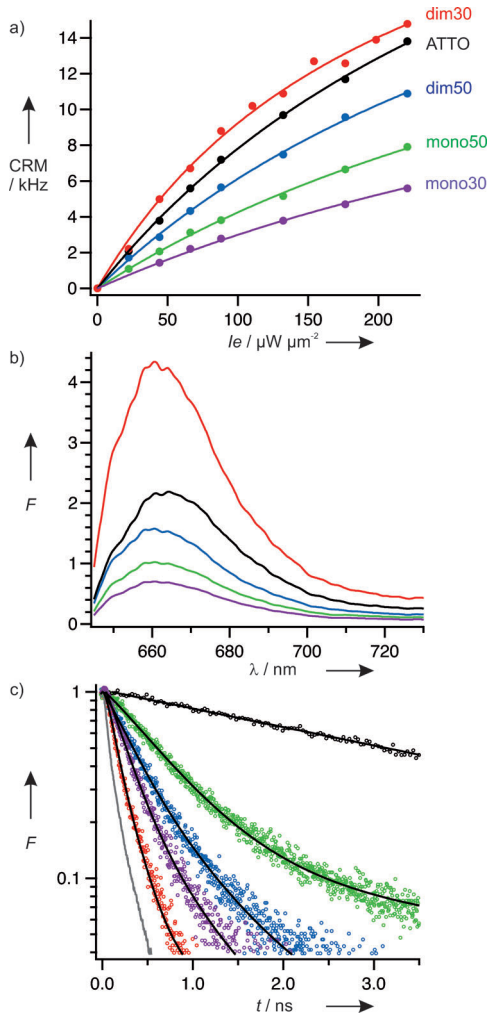

Figure 2. Count rate per molecule (CRM) as a function of a) the excitation intensity, b) fluorescence (*F*) spectra normalized per emitter, and c) normalized fluorescence decay traces of the reference ATTO sample (black), mono50 (green), mono30 (purple), dim50 (blue), and dim30 (red). Solid lines in (a) correspond to theoretical fit functions of the saturation curves. Solid black lines in (c) are fitted decay curves. Grey data points in (c) correspond to the instrument response function.

electronic eigenstates of the molecule as expected in a weak coupling regime. ATTO647N absorption and emission peaks are thus strongly red-shifted with respect to the plasmon resonance of DNA-templated 40 nm AuNP dimers around 560 nm (see the Supporting Information).

Figure 2c displays typical time-correlated fluorescence decay traces used to measure the fluorescence lifetimes τ given in Table 2. While the fluorescence decay of the reference and dim30 samples are fitted with a single exponential curve (convoluted with the instrument response function, see the Supporting Information), the numerical fitting of the decay traces are consistent with a 2.5% subpopulation of free dyes for the monomer samples and a 30% subpopulation of mono50 in dim50. The decay traces thus confirm the sample purities estimated by FCS and are in good agreement with cryo-EM measurements. Table 2 highlights the dramatic influence of AuNPs on the fluorescence lifetimes, which are reduced from 4.3 ns for the ATTO reference down to 65 ps for dim30. In the case of the dimer samples, these strong modifications are observed with similar luminescence signals compared to a reference ATTO sample. It is thus possible to design bright metal–organic emitters with sub-100 ps lifetimes using photonic engineering.

To go further and quantify the chromophore molar extinction coefficient ε and quantum yield ϕ we analyze the saturation curves of Figure 2a by considering a quantized two-level system. Under steady-state conditions, the detected count rate per molecule, CRM, is given by Equation (1),[27]

$$CRM = \kappa\,\phi\,\frac{\sigma\,I_e}{1 + I_e/I_{sat}} \qquad (1)$$

where κ is the collection efficiency, σ the excitation cross-section, I_e the excitation intensity, and I_{sat} the saturation intensity, which can be expressed as a function of the total decay rate $k_{tot} = 1/\tau$ as $I_{sat} = k_{tot}/\sigma$ (neglecting triplet contributions, as confirmed by the FCS curves). Fitting the curves in Figure 2a with Equation (1) allows us to infer the relative changes induced by the AuNPs on the excitation cross-section and quantum yield, respective to the ATTO reference. From these values and the tabulated photophysical properties of ATTO647N dyes, we estimate in Table 2 the values of the molecular extinction coefficients ε and quantum yields ϕ for hybrid gold–organic chromophores. Apart for mono50, all other samples feature absorption cross-sections and fluorescence quantum yields that are modified by over one order of magnitude. Surprisingly, the dim30 sample can be as bright as the ATTO reference, but with a quantum yield of only 1.6%, thanks to a much higher excitation cross-section that compensates for the quenching ohmic losses in the AuNPs.

To further confirm that our studied samples correspond to purified suspensions of AuNP monomers and dimers linked to one ATTO647N-modified DNA strand, we compare experimental luminescence lifetimes with theoretical estimates of τ. In practice, fluorescence lifetimes are estimated by computing the power dissipated by a point dipole in AuNP monomers and dimers using classical electromagnetic theory.[28,29] Since dye-modified DNA strands feature fixed[30] but uncontrolled molecular orientations, we take an isotropic distribution of the angle between the molecular transition dipole and the particles. The emitter–AuNP distances are set at 6.5 and 9.5 nm for the 30 bp and 50 bp linkers, in good agreement with cryo-EM and scattering spectroscopy.[20] With these distances, theoretical values of τ obtained with Mie theory are 574/182 ps for the 50/30 bp monomers and 198/69 ps for the 50/30 bp dimers, which are in excellent agreement with the experimental values given in Table 2.

Classical electromagnetic theory can also be used to highlight how brighter hybrid chromophores can be engineered.[28,29] In particular, the luminescence brightness strongly depends on the orientation of the molecular transition dipole with respect to the dimer axis.[21] If all molecules were oriented along the dimer axis, the theoretical enhancement factors are expected to be increased by a factor of about 3 with maximum ε and minimum τ. This would require rigid chemical linkers between dye molecules and one or two DNA

bases. Controlling molecular orientations in hybrid emitter–antenna systems appears essential to design bright ultrafast fluorescent nanostructures.

In conclusion, we have demonstrated that AuNP dimers can be used to electromagnetically engineer the photophysical properties of organic dyes, while preserving their solubility. These hybrid metal–organic emitters were fully characterized by their molar extinction coefficients, fluorescence lifetimes, quantum yields, and translational and rotational diffusion coefficients. In particular, 30 bp DNA-templated dimers feature absorption cross-sections and decay rates enhanced by more than one order of magnitude with respect to isolated dyes while producing high fluorescence count rates. These hybrid chromophores are bright emitters with lifetimes below 100 ps, quantum yields of a few percent, and large excitation cross-sections. Experimental results stand in good agreement with calculations based on classical electromagnetic theory which in turn indicates how the emitter brightness can be further optimized in rigid DNA-chromophore complexes with controlled molecular orientations. This work shows that by tuning the emission wavelength of the dye molecule with respect to the plasmon resonance, and by minimizing ohmic losses in the nanostructure, photonic engineering of luminescence will allow the development of unprecedented photophysical properties in hybrid metal–organic chromophores.

Experimental Section

Hybrid metal–organic chromophores were synthesized and purified using published procedures.[20,21] In brief, commercial 40 nm AuNPs (BBI, UK) are coated with a negatively charged phosphine ligand (BSPP, Strem Chemicals, USA) then rinsed and concentrated by centrifugation. 30 or 50 bases long trithiolated DNA strands (Fidelity Systems inc., USA) are effectively lengthened by thermal annealing with five consecutive 100 bases long PAGE-purified DNA strands (IDT DNA, USA). All DNA sequences are taken from previous published work.[20] The complementary sequences of the 30 and 50 bases long strands are commercially modified with one ATTO647N dye molecule on a central amine-modified base, and also lengthened with five 100 bases long strands. The phosphine coated AuNPs and lengthened DNA strands are left to react overnight in water with a 30 times excess of DNA at 30 mM NaCl. The phosphine ligand is replaced by adding an excess of short thiolated methyl-teminated ethylene glycol oligomers (Polypure, Norway) before particles functionalized with 0, 1. or 2 DNA strands are electrophoretically separated in a 1.5 % w/w agarose gel. Part of the monofunctionalized AuNPs (with one ATTO647N molecule) is hybridized to unmodified 30 or 50 bases long complementary strands to yield mono30 and mono50. The rest of the samples are hybridized to monofunctionalized AuNPs with the complementary strand (without dye molecule) to produce dim30 and dim50. Hybrization procedures are performed at 55 °C to remove the lengthening strands that are hybridized over 15 bps. Monomer and dimer samples are purified twice in electrophoresis (1.5 % w/w agarose) to remove free dye-modified DNA strands and monomers from dimer suspensions. The reference ATTO sample is obtained by annealing overnight the ATTO647N modified 50 bases long trithiolated strand to a nonthiolated complementary strand at 100 mM NaCl.

Experiments are performed with about 200 pM chromophore concentrations, on a custom developed confocal microscope using a 1.2 NA water immersion objective and linearly polarized 633 nm excitation (NA = numerical aperture). FCS measurements are performed under continuous-wave illumination by cross-correlating the signal from two avalanche photodiodes with a hardware correlator. Lifetime measurements are performed under picosecond pulsed illumination by a time-correlated single-photon counting module displaying 120 ps overall temporal resolution. Full details on the experimental setup, data analysis, and raw FCS data are given in the Supporting Information.

Theoretical calculations are performed using an in-house generalized Mie theory code.[29] The emission wavelength is set at 670 nm and the particle diameter at 40 nm. The refractive index of the surrounding medium is set at 1.335, while the dielectric constant of gold is tabulated from published data.[31] Theoretical fluorescence lifetime estimations are performed up to a multipolar order of 30 and by taking into account that the brightness depends on the molecular transition dipole orientation.

Received: July 26, 2012
Published online: October 4, 2012

Keywords: DNA · fluorescence · fluorescence correlation spectroscopy · nanoparticles · self-assembly

[1] J. Zyss, I. Ledoux, *Chem. Rev.* **1994**, *94*, 77.
[2] A. Mishra, R. K. Behera, P. K. Behera, B. K. Mishra, G. B. Behera, *Chem. Rev.* **2000**, *100*, 1973.
[3] O. Maury, H. Le Bozec, *Acc. Chem. Res.* **2005**, *38*, 691.
[4] J. R. Lakowicz, *Principles of Fluorescence Spectroscopy*, 4th ed., Springer, Berlin, **2006**.
[5] K. H. Drexhage, M. Fleck, H. Kuhn, F. P. Schafer, W. Sperling, *Ber. Bunsen-Ges.* **1966**, *70*, 1179.
[6] R. R. Chance, A. Prock, R. Silbey, *Adv. Chem. Phys.* **1978**, *37*, 1.
[7] P. Bharadwaj, B. Deutsch, L. Novotny, *Adv. Opt. Photonics* **2009**, *1*, 438.
[8] P. Anger, P. Bharadwaj, L. Novotny, *Phys. Rev. Lett.* **2006**, *96*, 113002.
[9] S. Kuhn, U. Hakanson, L. Rogobete, V. Sandoghdar, *Phys. Rev. Lett.* **2006**, *97*, 017402.
[10] J. R. Lakowicz, *Anal. Biochem.* **2005**, *337*, 171.
[11] K. Aslan, J. R. Lakowicz, C. D. Geddes, *Curr. Opin. Chem. Biol.* **2005**, *9*, 538.
[12] J. Seelig, K. Leslie, A. Renn, S. Kuhn, V. Jacobsen, M. van de Corput, C. Wyman, V. Sandoghdar, *Nano Lett.* **2007**, *7*, 685.
[13] J. Zhang, Y. Fu, M. H. Chowdhury, J. R. Lakowicz, *Nano Lett.* **2007**, *7*, 2101.
[14] A. Kinkhabwala, Z. Yu, F. S, Y. Avlasevich, K. Mullen, W. E. Moerner, *Nat. Photonics* **2009**, *3*, 654.
[15] H. Aouani, O. Mahboub, N. Bonod, E. Devaux, E. Popov, H. Rigneault, T. W. Ebbesen, J. Wenger, *Nano Lett.* **2011**, *11*, 637.
[16] K. Munechika, Y. Chen, A. F. Tillack, A. P. Kulkarni, I. Jen-La Plante, A. M. Munro, D. S. Ginger, *Nano Lett.* **2011**, *11*, 2725.
[17] T. Ming, L. Zhao, H. Chen, K. C. Woo, J. Wang, H.-Q. Lin, *Nano Lett.* **2011**, *11*, 2296.
[18] G. P. Acuna, M. Bucher, I. H. Stein, C. Steinhauer, A. Kuzyk, P. Holzmeister, R. Schreiber, A. Moroz, F. D. Stefani, T. Liedl, F. C. Simmel, P. Tinnefeld, *ACS Nano* **2012**, *6*, 3189.
[19] L. Novotny, N. van Hulst, *Nat. Photonics* **2011**, *5*, 83.
[20] M. P. Busson, B. Rolly, B. Stout, N. Bonod, E. Larquet, A. Polman, S. Bidault, *Nano Lett.* **2011**, *11*, 5060.
[21] M. P. Busson, B. Rolly, B. Stout, N. Bonod, S. Bidault, *Nat. Commun.* **2012**, *3*, 962.
[22] S. Derom, R. Vincent, A. Bouhelier, G. Colas des Francs, *EPL* **2012**, *98*, 47008.

[23] R. Rigler, E. S. Elson, *Fluorescence correlation spectroscopy, Theory and Applications*, Springer, Berlin, **2001**, p. 1.
[24] E. Haustein, P. Schwille, *Curr. Opin. Struct. Biol.* **2004**, *14*, 531.
[25] S. Maiti, U. Haupts, W. W. Webb, *Proc. Natl. Acad. Sci. USA* **1997**, *94*, 11753.
[26] C. M. Pieper, J. Enderlein, *Chem. Phys. Lett.* **2011**, *516*, 1.
[27] C. Zander, J. Enderlein, R. A. Keller, *Single-Molecule Detection in Solution—Methods and Applications*, Wiley-VCH, Weinheim, **2002**, p. 23.
[28] L. Rogobete, F. Kaminski, M. Agio, V. Sandoghdar, *Opt. Lett.* **2007**, *32*, 1623.
[29] A. Devilez, B. Stout, N. Bonod, *ACS Nano* **2010**, *4*, 3390.
[30] A. Kupstat, T. Ritschel, M. U. Kumke, *Bioconjugate Chem.* **2011**, *22*, 2546.
[31] P. B. Johnson, R. W. Christy, *Phys. Rev. B* **1972**, *6*, 4370.

